ALOS

K&C Initiative

An international science collaboration led by JAXA

Land-Atmosphere Carbon Exchange in Boreal Wetlands: Integration of ALOS PALSAR for Remote Sensing and Process Modeling

Kyle C. McDonald, Erika Podest, Ronny Schroeder Bruce Chapman (Jet Propulsion Lab, California Institute of Technology); Ted Bohn, Dennis Lettenmaier (University of Washington) Contact: kyle.c.mcdonald@jpl.nasa.gov

Summary

Changes in greenhouse gas emissions such as methane (CH4) and carbon dioxide (CO2) from high-latitude wetlands in a warming climate may have important implications for projections of global warming, due to the large amounts of carbon stored in high-latitude soils and the high greenhouse warming potential of methane. As much as 1/3 of global natural methane emissions come from high latitudes. Emissions of greenhouse gases, especially methane, are sensitive to hydrologic variables such as inundation that now can be observed via microwave remote sensing. We are applying a combination of large-scale hydrologic/biogeochemical models and remote sensing observations across the West Siberian lowlands to estimate soil moisture, inundation, and greenhouse gas fluxes. We have calibrated this framework using observed streamflow, inundation products derived from PALSAR and AMSR-E, and in situ water table and greenhouse gas emissions observations.

Modeling Approach

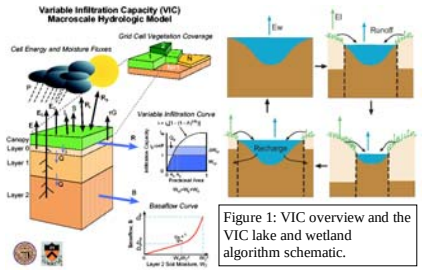

Figure 1: VIC overview and the VIC lake and wetland algorithm schematic.

Land Surface Hydrology Model

- Variable Infiltration Capacity (VIC) Model (Liang et al. 1994)
- Water and energy balance closure
- Macroscale: grid cells range from 10 to 100 km
- Statistical parameterizations of sub-grid variability in soil moisture, land cover
- Lake/wetland model (Bowling, 2002) handles changes in lake extent
- Grid cell average water table computed as sum of total column soil moisture deficit
- Extended to handle carbon cycling with Farquhar photosynthesis, plant respiration, and NPP from BETHY (Knorr, 2000)

Sub-grid Variability of Water Table and Inundation

- Uses topographic wetness index formulation from TOPMODEL (Beven and Kirkby, 1979)
- Relates local water table position to local topography and the average water table depth of the region

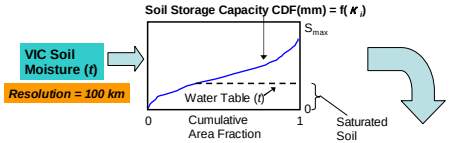

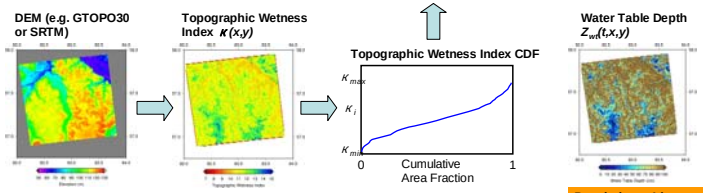

Methane Model

- Walter and Heimann (2000) with modifications described in Walter et al (2001a)
- soil methane production, and transport of methane by diffusion, ebullition, and through plants modeled explicitly
- methane production occurs in the anoxic soil from the bottom of the soil column to the water table
- methane production rate controlled by soil temperature and NPP (both from VIC)
- methane oxidation also taken into account

Model Framework

- VIC hydrologic model driven by (1) gridded meteorological forcings and (2) wetness index distribution from SRTM3 and GTOPO30 DEMs
- VIC produces daily Zwt distribution, Soil T, and NPP
- Distributed Zwt(x,y), SoilT, and NPP drive methane and soil respiration models, which produce CH4(x,y,t) and CO2(x,y,t)

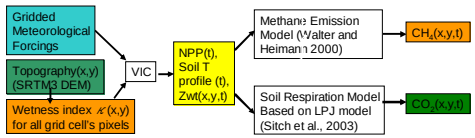

Wetlands Classification from ALOS PALSAR

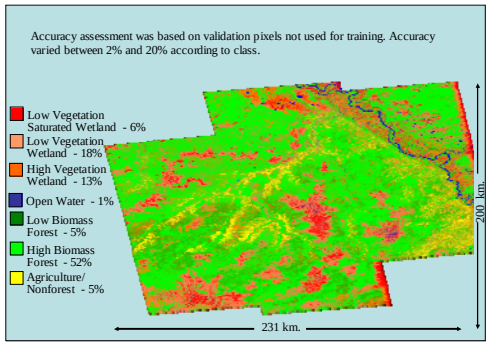

A decision tree classification based on the Random Forests approach was used to classify the SAR data. The ancillary datasets (described above and below right) were used within the classifier to support product generation. Application of the Random Forest approach for SAR-based classification was demonstrated previously in development of a wetlands map of Alaska using JERS datasets (below left). This was the first synoptic wetlands map for Alaska developed from a single remote sensing data source (Whitcomb et al 2009). Similar products are under development for several hydrologic basins in our NEESPI domain (shown at right).

Study Domain

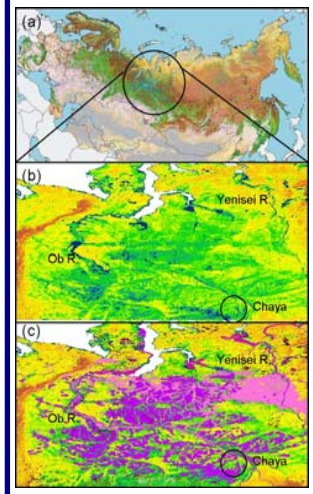

Fig. 1. Our current study domain, circled in panel (a), is the West Siberian Lowlands, home to a large portion of the world's wetlands. Panel (b) shows the topographic wetness index across this domain, derived from SRTM3 and GTOPO30 DEMs. Red = low wetness index, blue = high wetness index. Panel (c) overlays the wetland delineation of Lehner and Doll (2004). It can be seen that the spatial distribution of wetlands correlates strongly with high values of wetness index.

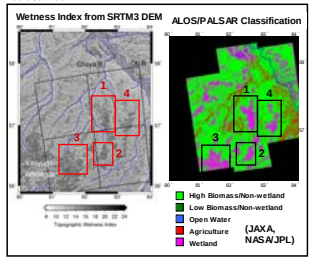

Fig. 2. Focus area: Chaya/Bakchar/Iksa watershed. We are running our modeling framework at a resolution of 100km (EASE grid equal-area polar projection) (grid cells outlined in panel (a)). Topography is supplied by the SRTM 30m UTM DEM. For comparison with simulations, and to calibrating the modeling framework, we have classified 12.5m UTM PALSAR imagery from the region (panel (b)), acquired in the summers of 2006-07. Classes of particular interest are: open water and saturated/inundated land (with emergent vegetation) (listed as "wetland" in the legend in panel (b)). To calibrate the water table parameterization, we have selected 4 regions of interest (ROIs), shown as numbered boxes in panels (a) and (b).

Model Calibration

We are calibrating the modeling framework using a combination of *in situ* and remotely-sensed observations:

1. Gauged streamflows in sub-basins covering 70% of the region, 1950-1970. These help constrain the depth of the simulated soil column, its drainage properties, and the relationship between topographic wetness index and water table depth.

2. Remotely-sensed observations of inundation, derived from Landsat, AMSR-E, and PALSAR imagery, 1970s through 2007. These help constrain lake drainage and the relationship between topographic wetness index and water table depth.

3. In situ measurements of CH4 and CO2 emissions at a small number of locations in the domain. These help constrain carbon cycle parameters but due to their scarcity, we will need to explore the responses over a range of plausible parameter values.

Figure 3. Simulated and observed inundation from ROIs in Figure 2.

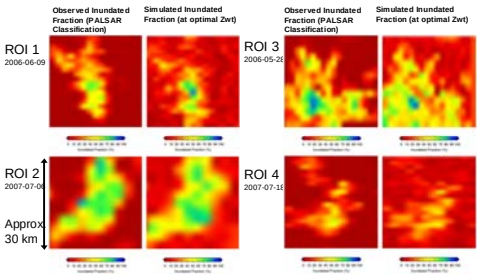

For each of the ROIs in fig. 2, we aggregated the remote sensing classifications up to 2700m resolution, computing the fraction of inundated 12.5m pixels in each 2700m "cell". Examples of observed inundation at each of the ROIs are shown in the first and third columns of fig. 3, along with acquisition dates.

Before analyzing topography, we first smoothed the DEM with a cutoff wavelength of 2100 m, to reduce noise in the DEM caused by its coarse (1 m) vertical resolution and the effects of scattered tree canopies on the DEM. Then we computed wetness index values at all 30 m pixels of the smoothed DEM.

For each ROI, we aggregated to 2700 m resolution, computing the fraction of 30 m DEM pixels having wetness index κ_i > threshold κ_i within each 2700 m cell, for a range of threshold κ_i values. For each κ_i value, we evaluated the bias: mean(fraction >= κ_i) - mean(fraction_inundated). We then selected the κ_i value for which bias was smallest as the "best" estimate for that ROI and date. Maps of fraction above threshold at each of the ROIs on the same dates as the observations are shown in the second and fourth columns of fig. 3. The strong correspondence between the spatial distributions of simulated and observed inundation is evident.

Comparison of PALSAR, Global Inundation, and Model Products

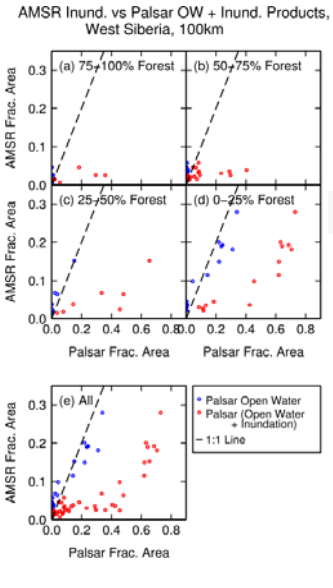

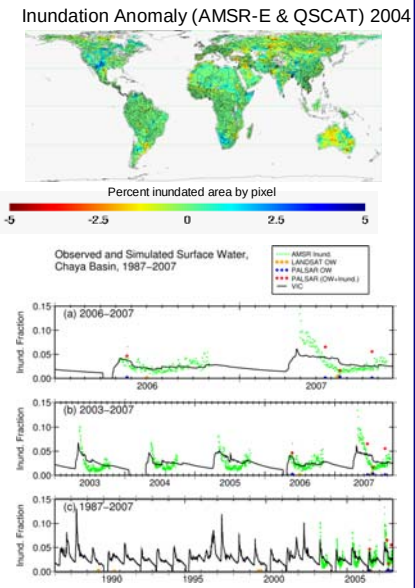

Jet Propulsion Laboratory

UNIVERSITY OF WASHINGTON

This work was carried out at the Jet Propulsion Laboratory, California Institute of Technology and at the University of Washington, under contract with the National Aeronautics and Space Administration. *This work has been undertaken in part within the framework of the JAXA ALOS Kyoto & Carbon Initiative. PALSAR data were provided by JAXA EORC.*